29th Congress of the International Council of the Aeronautical Sciences
St. Petersburg, Russia; September 7-12, 2014

# ROUGHNESS EFFECTS ON SWEPT-WING CROSSFLOW TRANSITION IN MODERATE FREE-STREAM TURBULENCE

**T.I. Saeed*, J.F. Morrison* and M.S. Mughal+**
***Department of Aeronautics, +Department of Mathematics, Imperial College London**

**Keywords:** *wing, roughness, turbulence, crossflow, transition*

## Abstract

*An experimental investigation of swept-wing crossflow transition is carried out, focussing on the effects of chord Reynolds number and direct roughness element height (spaced at the critical crossflow wavelength) in a moderate-level disturbance facility. Flow quality measurements performed in the wind tunnel indicate turbulence intensities of* $u'_{rms}/U_\infty = 0.14\%$ *and* $v'_{rms}/U_\infty = 0.20\%$*. The Reynolds numbers are* $Re_c = 1.3 \times 10^6$ *and* $Re_c = 1.6 \times 10^6$*. Despite the disturbance levels being indicative of travelling wave dominated crossflow, flow visualisation reveals that stationary crossflow is the dominant mode. Increased DRE height is shown through flow visualisation to advance transition, with boundary-layer velocity profiles showing mean-flow deformation and fluctuating-velocity spectra containing a high-frequency mode normally associated with stationary crossflow related secondary instability. Nevertheless, spectral information and unsteady disturbance profiles do indicate the travelling crossflow modes are excited, and that their disturbance amplitude increases with Reynolds number (as expected from linear stability theory) and with roughness height.*

## 1 Introduction

Despite there being no shortage of publications on the topic of swept-wing transition, both experimentally and computationally (see, for example, the reviews of [Bip99] and [SRW03]), there is still considerable interest in the area. This in part is driven by the need for more efficient aircraft, which in turn demand more accurate transition prediction tools [Gre08]. The $e^N$ method is the current industry standard. However its two obvious shortfalls are that it is unable to account for non-linearities in the flow and does not consider environmental disturbances [Mac84]. There is therefore renewed interest in developing techniques that capture all the necessary physics of the problem.

Ultimately, designers want to be able to predict the performance of an aircraft in flight. Flight tests are expensive, therefore extensive wind tunnel tests usually precede these. However, for boundary-layer stability problems, the conditions in a wind tunnel are not representative of flight. Recently [CSR08] measured disturbance levels of less than 0.05% at flight altitude. Most commercial, industrial, wind tunnels have disturbance levels in excess of 0.1% [KFA11]. Nevertheless, wind tunnel tests will always play an integral part in boundary-layer stability studies. Therefore, flow phenomena that arise inside a wind tunnel are still of interest.

There are four types of instability mechanisms that appear on swept wings: attachment line, streamwise, centrifugal, and crossflow. The focus of this study is the crossflow instability. [SRW03] provide a concise summary; briefly, this instability arises due to a secondary, spanwise flow in the three-dimensional boundary layer, and is connected with the in-plane curvature of the external-flow streamlines, as a result of the combined influences of sweep and pressure gradient. The crossflow velocity profile features an inflection point, which in turn leads to a basic inviscid instability mechanism.

The physical manifestation of this instability is a spanwise array of co-rotating vortices, whose axes are aligned approximately with the inviscid streamlines. The disturbance itself actually takes the form of counter-rotating vortices, with the dominant velocity component being in the streamwise direction i.e. weak $v'$ and $w'$ feed into $u'$. Here cartesian axes *x, y, z* are used for mean velocities *U, V, W* and the corresponding fluctuations *u', v', w'*. Depending on environmental conditions, amplified disturbances appear as stationary as well as travelling waves.

In general, the receptivity of 3D boundary layers are less well studied compared to 2D boundary layers. One of the first studies was by [DB96] who tested the sensitivity of the crossflow instability to a range of environmental conditions. They observed that, in contrast to T-S instabilities, sound has almost no effect on the crossflow while the effects of two-dimensional roughness and non-uniformities in the free-stream mean flow are also weak. [DB96] demonstrated that the growth of the crossflow disturbance has a complex dependence on initial conditions; specifically, three-dimensional roughness e.g. isolated or even an array of spanwise roughness elements, and free-stream turbulence (FST). However, investigations on the combined effects of surface roughness in moderate levels of free-stream turbulence and their influence on the travelling crossflow wave are few. This study therefore aims to provide more information on the receptivity, disturbance growth and transition of stationary and travelling crossflow waves in these conditions.

## 2 Background

For a number of years, receptivity models had only considered the sensitivity of stationary crossflows to surface roughness, and travelling wave sensitivity to free-stream turbulence. In response to this, [WSGG] conducted flow visualisation studies, and observed that for a swept wing with leading-edge distributed roughness of less than 0.5 $\mu$m in height and subjected to a free-stream disturbance level of 0.3%, stationary crossflow dominated transition was observed, with the emergence of a characteristic saw-tooth like transition front. In contrast, on insertion of a roughness array with subcritical spacing and height of 50 $\mu$m, transition moved forward significantly, with the transition front becoming more diffuse and uniform — characteristic of travelling-wave dominated transition. This provided an indication that roughness does not necessarily lead to the domination of stationary crossflow disturbances, and that specification of the turbulence level alone is not enough to predict which crossflow disturbance will dominate.

The experimental setup of [DB96] consisted of a swept-flat plate, with a displacement body giving the required surface pressure distribution, and tested in a tunnel with turbulence intensity of $Tu = 0.15\%$. The dependence of the crossflow mode on roughness shape, size, location and distribution was studied. The naturally distributed roughness heights were investigated through successive polishing of the plate: 1.8 $\mu$m, 6 $\mu$m and 40 $\mu$m. For the higher roughness height, earlier saturation of the stationary crossflow disturbance and an increase in its initial amplitude were observed. However, there was no noticeable effect on growth rate. In contrast, the influence of roughness height on the unsteady modes is said to be indirect, affected only by a secondary instability that arises due to earlier saturation of the stationary crossflow. Discrete, artificial, roughness elements were applied to the 1.8 $\mu$m polished surface. A two-dimensional roughness strip of constant width and height was seen to produce no appreciable difference in the spanwise distribution of $\bar{U}_s$ and $u_{rms}$ at $x/c = 0.90$, except at its spanwise extremities. [DB96] therefore concluded that it is *roughness-induced longitudinal vorticity* that is the important factor. Subsequently, roughness arrays were tested. It was found that the largest steady disturbance amplitude occurred with the roughness array placed close to the neutral point of the most-amplified stationary mode. Varying the roughness element diameter revealed maximum steady disturbance amplitudes for diameters equal to 30% of the spacing of the spanwise elements; [DB96] comment that this might have produced equally spaced roughness-generated vortices that are best

at triggering the crossflow vortex pattern best. Element spacings close to the naturally selected critical crossflow mode gave the largest steady disturbance amplitude. [DB96] do not provide information on how roughness diameter and element spacing affect the unsteady crossflow disturbance.

[DB96] increased FST from 0.15% to 0.27% by means of a turbulence generating grid in the same facility. This lead to a significant reduction in saturation amplitude of the stationary crossflow vortex, while the initial amplitude remained relatively unaffected, leading to the conclusion that the growth of steady disturbances is reduced in the presence of amplified unsteady disturbances. Similarly, the growth rate of the travelling wave instability reduces. However the initial disturbance amplitude increases significantly with FST. [DB96] asked whether differences in the spectral distribution of turbulent fluctuations lead to changes in the spectral content of the largest initial disturbance amplitude. Their findings, based on the spectral content of the streamwise fluctuations, suggested perhaps not, it rather depending more on the integrated turbulence intensity across all frequencies.

The receptivity of a swept-wing boundary layer to roughness element arrays (particularly with respect to height and spacing) was also recently examined by [HS11] in a low free-stream turbulence environment with $Tu = 0.02\%$. The investigation suggested that for this low turbulence level, crossflow disturbances appear more sensitive to roughness. Using the same model and facility, [DW13] explored in detail the sensitivity of stationary and travelling crossflow development to low free-stream turbulence and surface roughness. Three FST levels were investigated in the range $0.02\% \leq Tu \leq 0.2\%$; three roughness configurations were also tested: clean leading edge, sub-critically and critically spaced roughness arrays with heights of 12 $\mu$m and 14 $\mu$m, on a surface with baseline roughness of 0.2 $\mu$m rms. [DW13] quantified receptivity of the crossflow modes to environmental conditions by measuring disturbance amplitudes at 10% chord. The initial disturbance amplitude of the stationary crossflow mode was affected only by roughness, while it was largely unaffected by FST. The initial disturbance amplitude of the travelling wave however was affected by both, with even small increases at the lower end of the $Tu$ scale having a significant influence; furthermore, the unsteady mode was more receptive to FST in the presence of sub-critically spaced roughness elements. The argument for the latter observation is that sub-critically spaced elements produce a greater number of streamwise vortices (shed by the 3D roughness), which interact with FST in a more efficient manner. Nevertheless, critically spaced elements resulted in earlier transition compared to sub-critically spaced elements. At higher FST, the growth rate of the stationary crossflow decays, while that of the travelling wave increases. The latter observation is in contrast to that of [DB96] who record a decrease in the growth rate (despite a similar increase in initial amplitude). For the clean-leading-edge case, an increase in FST causes a substantial upstream movement in the transition location while in the presence of sub-critically spaced elements there was no noticeable effect. An increase in roughness height at higher FST also produced no visible effect either. Note that no detailed hot-wire measurements were conducted in order to provide quantitative explanations [Dow12].

[KFA11] experimentally investigated boundary-layer receptivity to free-stream turbulence for a smooth surface between $0.23\% \leq Tu \leq 0.58\%$, and surface roughness height $120\,\mu\text{m} \leq \text{k} \leq 420\,\mu\text{m}$ for the lowest value FST, over a swept flat plate. Over the range of turbulence levels explored, receptivity to FST was found to be linear for increasing turbulence intensity, and travelling modes start to dominate and inhibit the growth of stationary modes. Furthermore a threshold level of 0.25% was found to result in a lock-in of spanwise wavenumber, above which the turbulence length scale in the free-stream had no influence. In addition, the receptivity of the stationary crossflow mode to roughness height revealed that the initial disturbance amplitude increases non-linearly.

A number of Direct Numerical Simulations (DNS) give insight into the receptivity mechanisms that lead to crossflow disturbance growth.

One interesting set of studies was provided by [WK02] and [WK03], looking at oscillating surface mounted roughness elements exciting both stationary and travelling crossflows. These have also been studied experimentally [Bip99]. In the present study however, we are interested in free-stream vortical disturbances, and how they excite travelling waves in the presence of surface roughness. For that we refer to the studies of [SBH09], [SAB10] and [THH12].

[SBH09] model crossflow receptivity and disturbance evolution in a Falkner-Skan-Cooke boundary layer, with the computational domain beginning slightly downstream of the swept-flat-plate leading edge. The study investigates the influence of localised low-amplitude roughness arrays and weak free-stream vortical modes impinging on the boundary layer, and their combination. In agreement with other studies, roughness directly forces stationary crossflow modes and receptivity to this perturbation is most efficient when the elements are placed just upstream of the neutral point. The dependence of roughness receptivity on geometry is studied, and, provided the chordwise extension of the element is smaller than the chordwise wavelength of the most unstable steady mode, receptivity is dependent only on the spectral content of the element. However, non-linear effects appear only when the bump height is greater than 5% of the boundary-layer displacement thickness. The influence of FST is evaluated by studying the receptivity to individual continuous spectrum eigenmodes. Two factors that affect the receptivity of the boundary layer to free-stream vortical disturbances are: 1) whether or not these modes are able to penetrate the boundary layer effectively, and 2) how quickly they decay. The most penetrating modes are identified as quasi-2D waves, which take the form of large horizontal structures with scales larger than the most unstable waves. Direct excitation of travelling waves requires that the external perturbation have a matching wavenumber and frequency, in order to set up a resonance. Free-stream disturbances, in general, have different length scales to that of the unstable eigenmodes in the boundary layer. A scale-conversion process is said to facilitate the direct receptivity mechanism. This requires rapid mean-flow changes, for example in the strongly developing region at the leading edge or around a surface protrusion such as wall roughness. Non-parallel flow effects are therefore important. When there is a combination of free-stream vortical modes and surface roughness, [SBH09] describe two possible receptivity mechanisms: 1) the direct mechanisms already discussed, which result in unstable steady and unsteady modes that interact and force an unsteady amplifying wave; or 2) unstable steady modes, excited by the roughness element, interacting with stable unsteady modes that are not directly coupled with the free-stream: this mechanism is said to be due to a scattering of the vortical modes on the roughness elements. The receptivity coefficients of 2) are seen to be much lower than 1), and so it is concluded that mechanism 1) is responsible for unsteady eigenmode growth in low-disturbance environments.

[SAB10] take the modelling of combined receptivity further than [SBH09] with a more complex model for the free-stream vortical disturbance, which is made up of a superposition of modes from the continuous spectrum; also, they consider a localised roughness strip with spanwise random height distribution, which excites a number of steady modes. Turbulence levels over a range corresponding to flight conditions and turbomachinary applications are considered, $0.17\% \leq Tu \leq 5.06\%$. As in the experimental observations of [KFA11], receptivity to free-stream turbulence is seen to be linear; however, travelling wave disturbance evolution is non-linear for $Tu > 2.53\%$, and is most likely to be due to forcing among low-frequency unsteady modes. Downstream modes develop independently of the free-stream turbulence, due to the localised scale-conversion process that takes place around the leading edge. The spacing of the instabilities decreases with downstream distance, and is seen to be independent of turbulence level for $Tu < 1.69\%$, but decrease at a faster rate for higher values of FST. Just upstream of transition, the spacing is seen to increase before decreasing again. For FST in the presence of roughness, there is a critical range of turbulence level for a given roughness height above which travelling waves

become the dominant crossflow mode. The total disturbance amplitude is predicted by summing the growths of the stationary and travelling waves calculated independently. Therefore, the interaction between the two mode types appears negligible.

[THH12] perform more sophisticated DNS by modelling a swept-wing geometry and examining impinging vortical disturbances upstream of the leading edge on a smooth surface. The optimal vortical disturbance takes the form of a steady free-stream disturbance, which exhibits minor streamwise vorticity with a streak component that penetrates throughout the boundary layer. The optimal surface roughness for stationary crossflows takes the form of a streamwise-wavy wall.

The motivation for the present study is to contribute further to the understanding of receptivity due to the combined effects of surface roughness and free-stream turbulence. A survey of previous work, both experimental and DNS, lead to a number of questions:

1) The DNS studies of [SBH09], [SAB10] and [THH12] indicate that non-parallel flow, in regions of high-curvature such as around the leading edge or a surface irregularity, facilitates the scale-conversion process required to initiate a resonance between free-stream vortical disturbances and instability modes within the boundary layer. [DB96] examined the influence of a roughness strip on both steady and unsteady modes by measuring disturbance amplitudes far downstream, and concluded that it is longitudinal vorticity generated by 3D roughness which facilitates the receptivity mechanism, not the surface irregularity due to the presence of the roughness itself. This is further supported by the observations of [DW13] where the initial disturbance amplitude of the unsteady mode was seen to be higher for sub-critically spaced elements compared to critically spaced elements. They argue that this is due to the presence of more roughness-generated vortices inside the boundary layer. We shall investigate this further by quantifying the initial disturbance amplitude of the travelling wave for a variety of roughness configurations and geometries, including both strips and arrays.

2) The experiment of [DB96] illustrates the dominance of lateral fluctuations, $v'$ and $w'$, compared to streamwise, $u'$; they comment that all three components should therefore be considered when evaluating the overall disturbance intensity. They examine the spectral content of the streamwise component for a range of free-stream turbulence levels, and see that around the frequency of the travelling wave instability there is no significant difference. They conclude that it is the integrated turbulence level across all frequencies that is important. This observation supports the scale-conversion mechanism described in the DNS studies. It would however be useful to have information regarding the spectral distributions of the lateral components. It would then allow us to further understand the role played by the lateral disturbance components. It is therefore proposed in this study that the effects of FST anisotropy be investigated further.

In this study we outline initial investigations of the effects of roughness receptivity in moderate levels of free-stream turbulence on crossflow transition and disturbance growth. Discrete roughness arrays are utilised to excite critical crossflow modes, and their heights increased in order to investigate the influence on crossflow transition and whether or not it results in the dominance of a particular crossflow mode. Reynolds number effects are also investigated. The paper provides an overview of the experimental facility and the results of flow visualisation and boundary-layer hot-wire measurements.

## 3 Experimental facility and setup

In this section the wind-tunnel facility in which the measurements are conducted, the swept-wing model, the instrumentation and data acquisition technique used and the Direct Roughness Element (DRE) array used to trigger crossflow modes are described.

### 3.1 Wind tunnel

The experiments are performed in the Honda wind tunnel at the Department of Aeronautics, Imperial College London. It is a closed-loop fa-

cility that has a working test-section of 3 m x 1.5 m x 9 m and can attain flow speeds of up to 40 m/s. The tunnel has a mild contraction ratio of 3.6:1. It features one honeycomb and one turbulence reducing screen. The tunnel does not have active temperature control, but velocity feedback is used to maintain a constant Reynolds number.

### 3.2 Swept-wing model

The AERAST wing model is provided by Airbus; it was specifically designed to enhance the growth of the crossflow instability for experimental purposes in the ONERA F2 tunnel [SS09]. This is achieved with a pressure minimum at 71% chord and a wing sweep $\Lambda = 40^{\circ}$; the leading-edge radius and ellipse aspect ratio combination satisfactorily avoid attachment-line instability.

The wing section is a 0.8 m chord model with a span of 1.2 m and constructed from aluminium. The leading 10% of chord on the suction surface (the test side) is hand polished to a surface finish of 0.06 $\mu$m rms, measured using a Mitotoyo profilometer. Downstream, where the quality of surface finish is less important for stability experiments, the surface is sprayed-painted black to facilitate flow visualisation techniques. The model has streamwise rows of pressure ports, each with 49 tappings, at three span-wise locations: 25%, 50% and 75% span. These pressure ports allow measurement of the pressure distribution in the streamwise direction. The wing has a design root incidence of $-2.15^{\circ}$ at the root, with a tip-down linear twist of $1.5^{\circ}$.

The wing is mounted vertically in the wind tunnel as shown in Fig. 1. Its lateral position is between 0.38 and 0.45 unit span, to avoid vortical modes induced by corner vortices that form as a result of the rectangular cross section [TFY07], and also to avoid the weak vertical shear layer induced by a splitter plate which separates two contra-rotating fans. The model also has a boundary-layer splitter plate to avoid turbulence contamination from the tunnel floor along the wing leading edge.

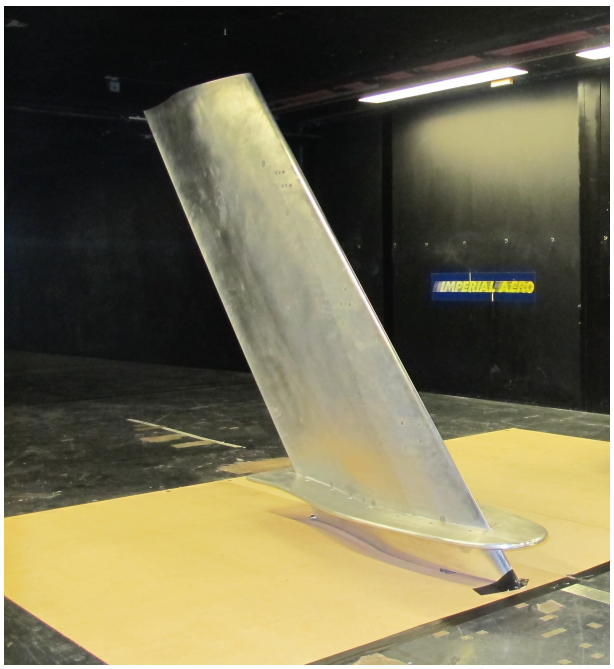


**Fig. 1** AERAST wing as mounted in Honda tunnel.

### 3.3 Instrumentation and data acquisition

Velocity measurements are performed using constant-temperature hot-wire anemometry to quantify the free-stream disturbance of the wind tunnel and for boundary-layer measurements. Both 5 $\mu$m diameter straight-single- and X-wire probes are used for the former, while a 5 $\mu$m boundary-layer probe is used for the latter. The anemometer is a Dantec Dynamics Streamline system. A 16-bit analogue-to-digital converter board is used for signal acquisition. Calibration of the hot wire is performed against a Pitot-static tube connected to a Furness FCO510 manometer. Hot-wire measurements are temperature compensated following the method detailed in [Bru96]. A bespoke traverse mechanism that allows for highly accurate probe location is used for surface-normal traverses.

To determine the location and pattern of the transition front, and crossflow vortex wavelength, flow visualisation is conducted using a sublimation technique. This consists of a spray-deposited layer of “china clay" for contrast, followed by a further spay deposition of methyl salicylate (“wintergreen"): the preferential rates of evaporation distinguishing laminar (dark regions) and

turbulent (light regions) regions. The test surface is sprayed black to help distinguish between the two regions.

### 3.4 DRE arrays

Appliqué roughness elements printed on a dry-ink transfer sheet, supplied by Redd Europe Ltd, are used. For the initial investigations presented in this paper, circular discrete roughness elements (DREs) of 2.8 mm diameter with a spacing of 6.3 mm are utilised — see Sec. 4. The DRE array is applied over 50% of the model span, with the measurement zone located between 50% – 75% span. The elements are placed just upstream of the neutral point at 1.8% chord — see Sec. 4. Element heights are increased by applying additional layers of DRE to the original layer: one layer gives $k = 12\,\mu$m and two layers gives $k = 24\,\mu$m. For consistency with recent experiments in the literature, the notation $[k|\lambda|d]$ is used to describe roughness array configurations, where $k$ has units of microns and $\lambda$ and d have units of millimetres.

## 4 Experiment design

### 4.1 Wing incidence

The swept-wing model was originally designed for $Re_c = 3 \times 10^6$ ([SS09]). Preliminary flow-visualisation investigations showed that crossflow transition was only attainable in the Honda tunnel when run at maximum speed, which gives a Reynolds number still much lower than the design value. Practically, such a test condition is undesirable because of wind tunnel heating effects and probe vibration issues. To overcome this, the crossflow instability was further excited by increasing the negative root-incidence of the wing to -4.5°.

A chordwise pressure distribution at $Re_c = 1.3 \times 10^6$ is shown in Fig. 2. The coefficient of pressure is computed using:

$$C_p = \frac{p - p_\infty}{\frac{1}{2}\rho U_\infty^2}, \qquad (1)$$

where $p$ is measured using a CANDaq pressure scanner, and the reference pressure, $P_\infty$, is acquired using the static port on a Pitot-static tube. The pressure measurements show little spanwise variation over the first 70% of chord. The pressure measurements suggest that there is no separation in the region of adverse pressure toward the wing trailing edge; this is confirmed further by flow visualisation.

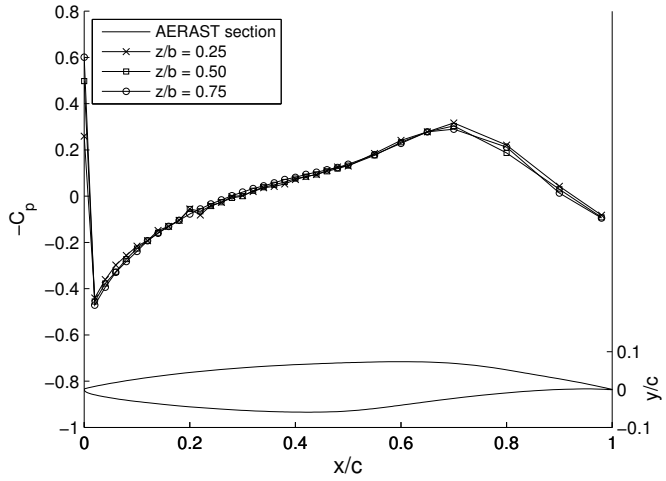


**Fig. 2** Pressure distributions at $Re_c = 1.3 \times 10^6, \alpha = -4.5°$.

### 4.2 Reynolds number

In selecting the Reynolds number several factors must be considered. Practically, if it is too high then wind tunnel heating effects can be substantial, and the transition location can be too far forward to conduct a detailed study of disturbance growth. With a lower Reynolds number, the boundary layer is thicker, but the disturbance growth may not be large enough to generate significant crossflow ([CRS96]).

To aid in selecting a test Reynolds number, linear stability calculations were performed using CoPSE ([MA13]). Though non-linear effects are important in crossflow dominated flows, Linear Stability Theory (LST) provides valuable insight into the relative growth of modes as well as information on the most unstable modes ([CRS96]).

Linear stability calculations were performed using experimentally determined pressure distributions for two chord Reynolds numbers: $Re_c = 1.3 \times 10^6$ and $Re_c = 1.6 \times 10^6$. The envelope

of $N$ factors for stationary crossflows and travelling waves is presented in Fig. 3. Consistent with LST, travelling waves have higher $N$ factors and grow at a faster rate than stationary crossflows ([Mac84]). The $N$ factors are high enough for the crossflow instability to be measurable, whilst low enough to avoid early transition. The neutral point for both Reynolds number case is located at approximately $x/c = 0.018$.

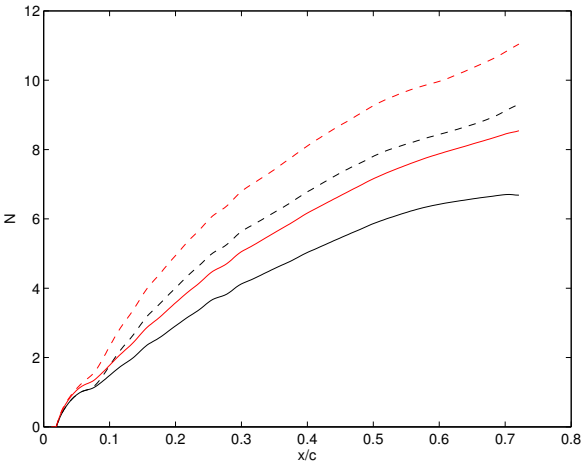


**Fig. 3** Envelope of $N$ factors for stationary (solid) and travelling (dashed) crossflow modes, $Re_c = 1.3 \times 10^6$ (black) and $Re_c = 1.6 \times 10^6$ (red).

### 4.3 DRE array configuration

The distribution of critical wavenumbers ($\beta$) for stationary and travelling crossflow modes is shown in Fig. 4. From this we can deduce that the critical wavenumber is between 900 /m and 1100 /m for the two Reynolds number cases. For this study, a value $\beta = 1000$ /m was used for both Reynolds number cases for controlled crossflow mode excitation; a DRE pitch of $2\pi/\beta = 6.3$ mm is chosen. The element diameter is set at 2.8 mm, between the recommended value of 40% – 50% element spacing ([Dow12]).

Figure 5 shows the distribution of critical travelling wave frequencies in the chordwise direction. Upstream of 10% chord higher frequencies of the travelling mode dominate; however as the disturbances evolve the frequency decreases. At 30% chord, the travelling wave frequencies

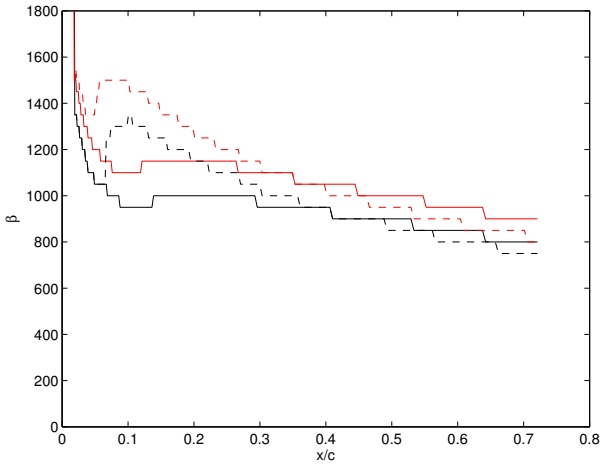


**Fig. 4** Envelope of wave numbers for stationary (solid) and travelling (dashed) crossflow modes, $Re_c = 1.3 \times 10^6$ (black) and $Re_c = 1.6 \times 10^6$ (red).

are 300 Hz – 400 Hz, while at 55% chord the frequencies are 200 Hz – 350 Hz.

## 5 Results

### 5.1 Free-stream measurements

Flow quality measurements were conducted in an empty wind tunnel, at the same streamwise position as where the wing model is located. The free-stream turbulence is characterised using hot-wire anemometry. All signals are acquired using a low-pass cut-off filter frequency of 10 kHz that is half the sample rate. Measurements are presented here at a tunnel speed of 25 m/s, which is in the operating range of the present experiments.

The velocity-fluctuation spectra for the streamwise ($u'$) and vertical ($v'$) components are shown in Fig. 6. The spectra are characteristic of a moderate-level turbulence facility in that the power distribution is broad. Both spectra show that a significant amount of power appears in the fluctuations for $f < 10$ Hz. This is similar to the observations of [DW13], who attribute such a feature to low-frequency oscillations that are correlated across a streamwise plane, and subsequently inflate the rms fluctuating values.

These low-frequency disturbances are attributed to sound (or pressure) induced veloc-

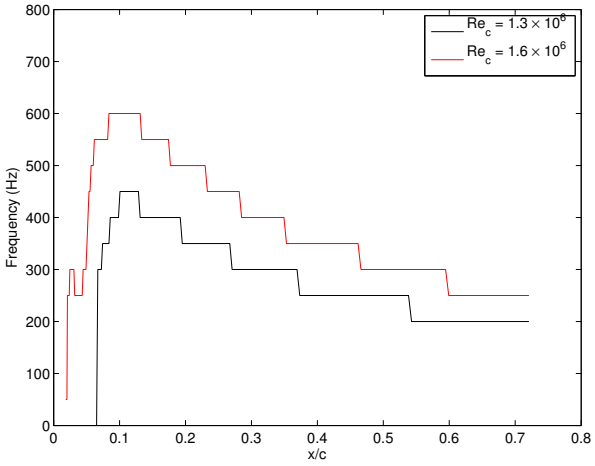


**Fig. 5** Distribution of critical travelling wave frequencies.

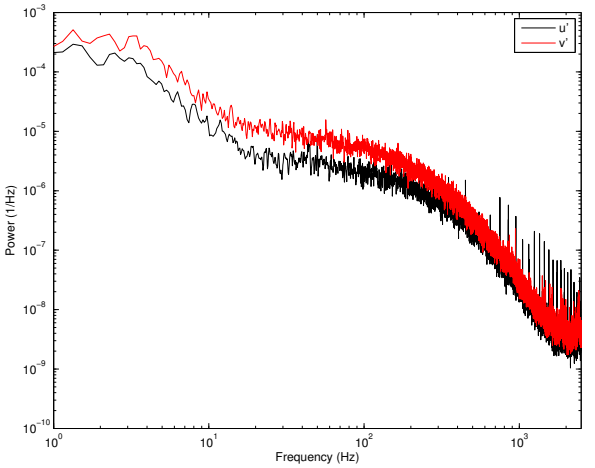


**Fig. 6** Free-stream fluctuating velocity-spectra, $U_\infty = 25$ m/s.

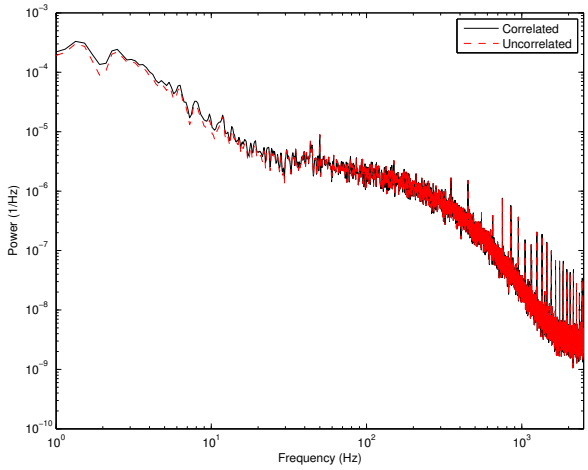


**Fig. 7** Comparison of streamwise fluctuating-velocity spectra computed with a sound/turbulence separation technique (uncorrelated) and without (correlated), $U_\infty = 25$ m/s.

ity fluctuations that do not influence crossflow instability. A sound/turbulence separation technique recommended by [TFY07], which is developed by [NGW96], is followed here. The spectra of the streamwise fluctuating-velocity component for the correlated (total disturbance) and uncorrelated (separated vortical disturbance) signals is shown in Fig. 7. There appears to be little correlation.

Flow quality measurements conducted by [LJ02] at KTH revealed that up to 50% of the fluctuating velocity is due to low-frequency oscillations. They propose a high-pass cut-off frequency given by $f_{HP} = U_\infty/\Lambda_L$, where $\Lambda_L$ is equal to the sum of the tunnel side wall lengths, as only disturbances that are of the scale of the wind-tunnel cross section are of importance. For the Honda tunnel $\Lambda = 4.5$ m, therefore, for a speed of 25 m/s, $f_{HP} = 5.6$ Hz.

Table 1 summarises the disturbance intensities for various high-pass filter frequencies. We see that the uncorrelated signal is all but identical to the correlated signal for both streamwise and vertical components. For consistency with [DW13] and other research published by TAMU, values for a passband of 1 Hz – 10 kHz is provided; in this instance $u'_{rms}/U_\infty = 0.18\%$ and

$v'_{rms}/U_\infty = 0.26\%$. Following [LJ02] $u'_{rms}/U_\infty = 0.14\%$ and $v'_{rms}/U_\infty = 0.20\%$.

| | | $u'_{rms}/U_\infty$ (%) | $v'_{rms}/U_\infty$ (%) |
|---|---|---|---|
| No HP | Correlated | 0.2334 | 0.2731 |
| | Uncorrelated | 0.2182 | 0.2731 |
| HP = 1 Hz | Correlated | 0.1784 | 0.2639 |
| | Uncorrelated | 0.1782 | 0.2639 |
| HP = 5.6 Hz | Correlated | 0.1362 | 0.2035 |
| | Uncorrelated | 0.1362 | 0.2035 |

**Table 1** Summary of turbulence levels measured at $U_\infty = 25$ m/s. A low-pass frequency of 10 kHz is applied for all values given.

## 5.2 Flow visualisation

Figure 8 shows the effect of increasing DRE height at $Re_c = 1.3 \times 10^6$. With a clean leading edge, the stationary crossflow vortex striations are visible; the measured wavelength is approximately 6 mm. The stationary vortices are persistent downstream of 60% chord, beyond the pressure minimum, in the region of adverse pressure gradient. The transition front is straight and uniform, suggesting that transition is T-S dominated. With a DRE height of 12 $\mu$m, the stationary crossflow vortex striations are still apparent. However the transition front has moved upstream to around 60% chord; the pattern is also more jagged. Increasing DRE height to 24 $\mu$m further influences the transition location, moving upstream to around 45% chord.

At $Re_c = 1.6 \times 10^6$, we see in Fig. 9 that for the clean leading edge case the transition front is sawtooth-like and is between 55% – 60% chord. Increasing roughness height to 12 $\mu$m the transition front is more uniform and moves further upstream to around 50% chord. At a DRE height of 24 $\mu$m the transition front moves to 40% chord; the crossflow vortex striations are less visible and the transition front is also more diffuse.

## 5.3 Boundary-layer measurements

The physical limitations in the hot-wire traverse system require that measurements are obtained in the cartesian coordinate system which is consistent with the tunnel geometry. The coordinate

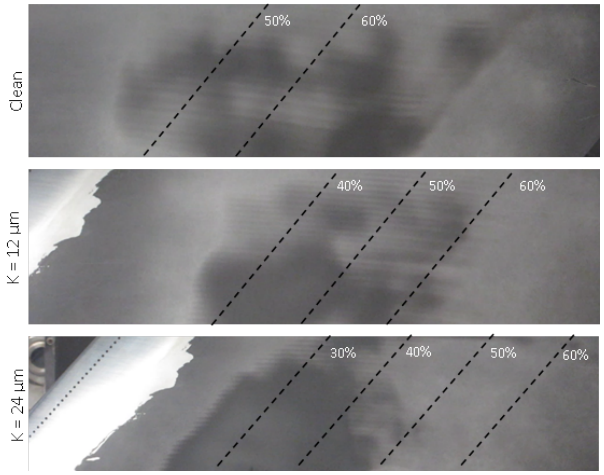


**Fig. 8** Surface flow visualisation at $Re_c = 1.3 \times 10^6$ for three roughness case: clean leading edge, $k = 12$ $\mu$m and $k = 24$ $\mu$m.

system of [WS05] is followed, where: $X$ is parallel to the free-stream-flow direction, $Y$ is normal to the wall of the test section and $z$ is parallel to the model leading edge. Consequently, velocities in the streamline-oriented coordinate system are measured as projections; this requires computational results be transformed to the same coordinate system for comparison ([WS05]). The minimum step size in the streamwise and wall-normal directions of the traverse system are $\Delta X = 0.1$ mm and $\Delta Y = 2.5$ $\mu$m, respectively.

The boundary-layer probe is adjusted so that the element is parallel to the local surface. The wire is moved to the boundary-layer edge and the scan started. Points are sampled at 50 kHz and for a duration of 10 seconds. A low-pass filter of 10 kHz is applied through the Dantec Streamline unit.

For each profile, there are approximately 75 measurement points inside the boundary layer and 25 points extending into the free stream. To avoid cooling effects between the wire and the aluminium surface, boundary-layer scans do not extend below a value of $U(Y,z)/U_e < 0.2$; the wall position is subsequently determined by extrapolating a second-order polynomial fit between $0.3 < U(Y,z)/U_e < 0.5$ and the surface. Therefore, the surface location can be determined from the measurements. This approach is similar to that of others — see for example [Hun11].

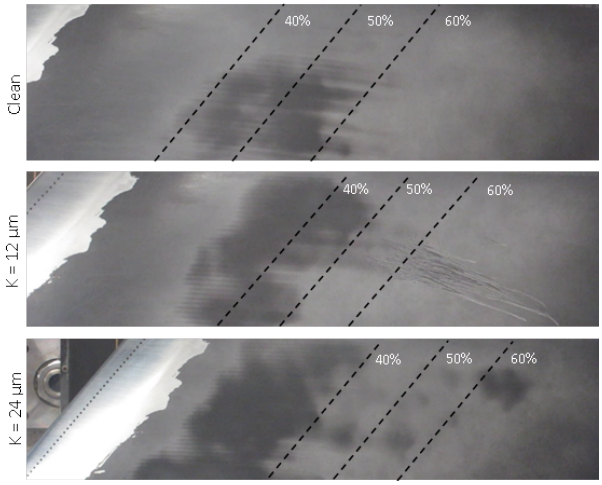


**Fig. 9** Surface flow visualisation at $Re_c = 1.6 \times 10^6$ for three roughness case: clean leading edge, $k = 12$ $\mu$m and $k = 24$ $\mu$m.

For the present investigation, measurement resolution is restricted to a single boundary-layer scan at a number of chordwise positions. Results are presented for the two chord Reynolds numbers and two DRE heights; baseline measurements for a clean leading edge are unavailable. Spectral information is presented at a wall-normal distance corresponding to a boundary-layer mean velocity ratio $U(Y)/U_e = 0.30$. Unsteady disturbance profiles are band-pass filtered between 50 Hz – 500 Hz to capture travelling wave growth.

### *5.3.1* $Re_c = 1.3 \times 10^6$

Figure 10 shows the velocity spectra at several chordwise positions. Comparison of spectra at 30% and 55% chord shows that for frequencies above 1 kHz, the latter has a higher level of power distributed over a broader range of frequencies; at lower frequencies, the former shows distinct peaks between 50 Hz – 250 Hz, while the latter only has a distinct peak at 250 Hz. This is consistent with the linear stability analysis of the travelling crossflow presented in Sec. 4. Oscillations below 50 Hz are suspected to be due to probe vibration. The peak in the spectrum taken at 30% chord at around 800 Hz does not appear in the LST calculations; such a peak was reported in the work of [WS05] and was attributed to a streamwise T-S instability. Further downstream at $x/c = 0.50$ the power spectrum is positioned between the two extremes discussed. However a peak appears at around 4 kHz. As this is just upstream of the transition front, shown in Fig. 8, it is suspected that this maybe a high-frequency secondary instability attributed to the mean flow modifications that arise due to the growth of the stationary crossflow vortex.

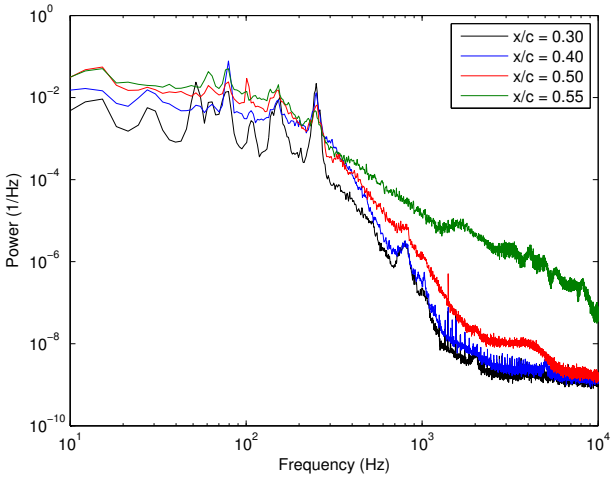


**Fig. 10** Fluctuating-velocity spectra, $Re_c = 1.3 \times 10^6$, [12|6.3|2.8] roughness.

Figure 11 shows several boundary-layer velocity profiles. At $x/c = 0.30$ the profile is distinctly laminar; the profile at $x/c = 0.40$ is similar but thicker, yet still characteristically laminar; at x/c = 0.50 however we see start to see a kink in the profile for $U(Y)/U_e > 0.8$; at $x/c = 0.55$ an inflectional profile appears. These observations are consistent with those made of the velocity-fluctuation spectra in Fig. 10.

With only a single velocity profile at each chordwise position, we are unable to determine the disturbance amplitude of the stationary crossflow. We are however able to extract unsteady disturbance velocity information. In a low turbulence environment, we expect the unsteady disturbance profiles to be of low amplitude, as shown in the study of [DW13]. Mode shapes of $u'_{rms}$ in the travelling mode passband (computed using frequency band integration of $u'$) is shown in Fig. 12. The maximum unsteady disturbance amplitude at $x/c = 0.40$ is around 1.5 times that at $x/c = 0.30$; the subsequent increase in max-

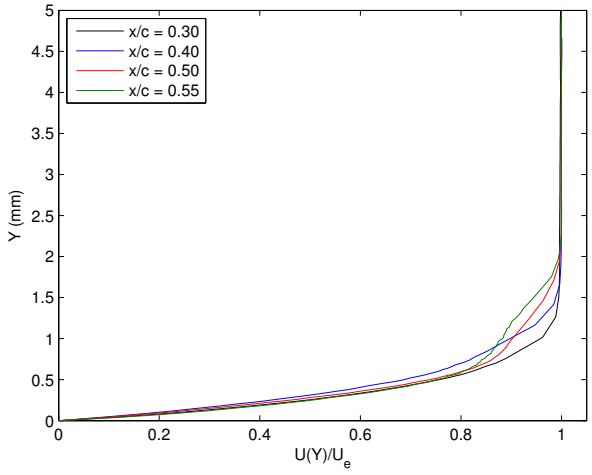


**Fig. 11** Boundary-layer velocity profiles, $Re_c = 1.3 \times 10^6$, [12|6.3|2.8] roughness.

imum disturbance amplitude is less pronounced at successive chordwise locations, suggesting the growth of the travelling disturbance is plateauing, as is consistent with LST. The disturbance amplitudes are of the same order as measured by [DW13], $0.02 < u'_{rms}/U_e < 0.04$.

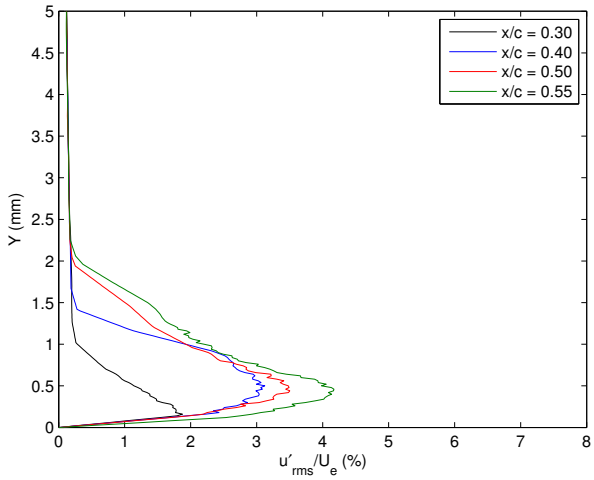


**Fig. 12** Unsteady disturbance profiles in the travelling-wave passband (50 – 500 Hz), $Re_c = 1.3 \times 10^6$, [12|6.3|2.8] roughness.

Increasing DRE height to 24 $\mu$m, the velocity spectra in Fig. 13 show the same characteristic features as at the lower DRE height. The high-frequency peak at 4 kHz is present in the spectra recorded at $x/c = 0.40$, but is more pronounced. This could be due to stronger stationary crossflow vortex growth and subsequently greater modification of the mean flow. In contrast, the unsteady disturbance profiles shown in Fig. 14 suggests that the travelling mode continues to grow downstream.

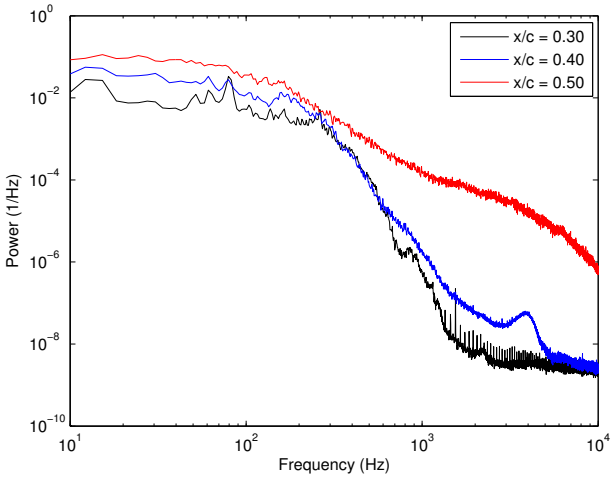


**Fig. 13** Fluctuating-velocity spectra, $Re_c = 1.3 \times 10^6$, [24|6.3|2.8] roughness.

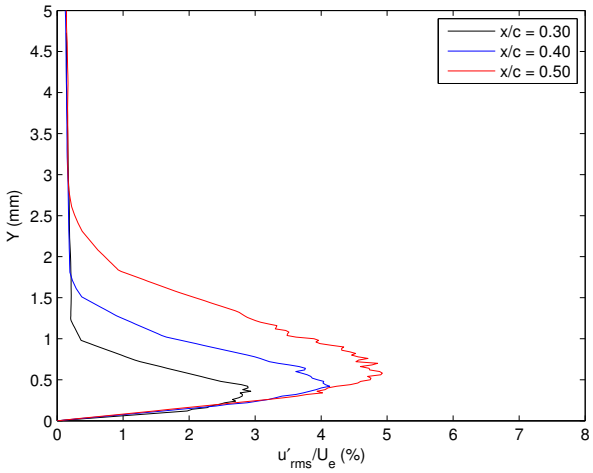


**Fig. 14** Unsteady disturbance profiles in the travelling-wave passband (50 – 500 Hz), $Re_c = 1.3 \times 10^6$, [24|6.3|2.8] roughness.

To compare the influence of DRE height, consider the velocity spectra measured at $x/c = 0.30$ in Fig. 15. Here we see that the power is distributed over a greater range of frequencies and is an order of magnitude higher. The suspected streamwise instability at about 800 Hz is

still present, but less distinct. Perhaps the increased roughness height leads to a more efficient receptivity mechanism that excites all travelling wave modes, leading to the broader power distribution spectrum. Figure 16 shows that the maximum unsteady disturbance amplitude increases by 1.5 times and has a wider profile.

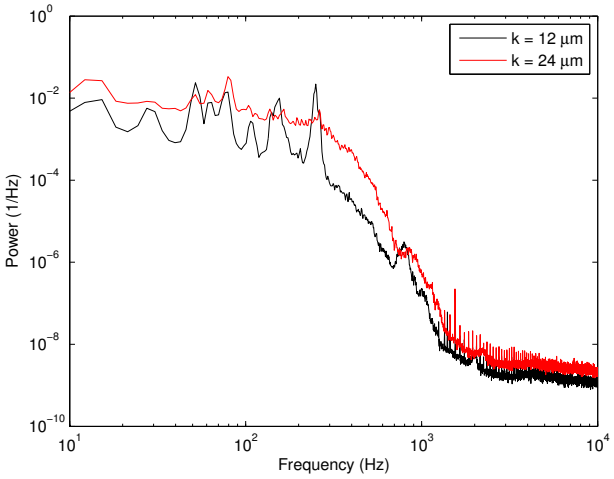


**Fig. 15** Fluctuating-velocity spectra, $Re_c = 1.3 \times 10^6$, $x/c = 0.30$.

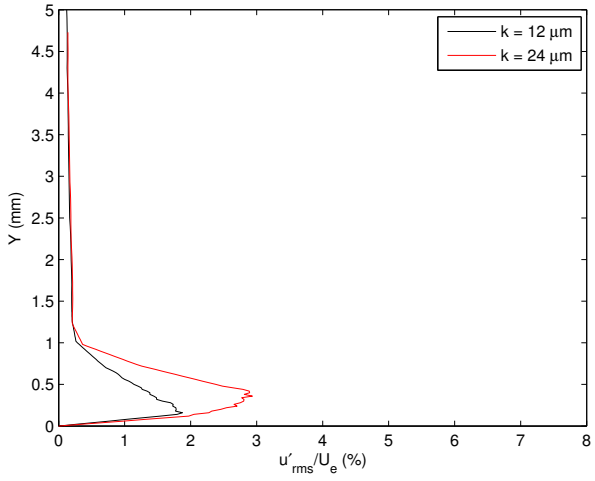


**Fig. 16** Unsteady disturbance profiles in the travelling-wave passband (50 – 500 Hz), $Re_c = 1.3 \times 10^6$, $x/c = 0.30$.

### *5.3.2* $Re_c = 1.6 \times 10^6$

Figure 17 shows the velocity spectrum for $k = 12$ $\mu$m. In many aspects it is similar to Fig. 10, for the lower Reynolds number case; however, the features begin to arise further upstream, as we would expect from the flow visualisation image of Fig. 9. At $x/c = 0.30$ the low-frequency peaks, most probably corresponding to the travelling modes, are apparent. However, the suspected streamwise instability at the higher frequency is no longer visible, and is probably due to the stronger crossflow instability. At $x/c = 0.40$ there are additional peaks at higher frequencies of around 2 kHz and 4 kHz, which are most probably secondary instabilities given the measurements are close to the transition front. At $x/c = 0.50$ where we expect from flow visualisation the flow to have transitioned, we see a greater level of power distributed across a broad range of high frequencies.

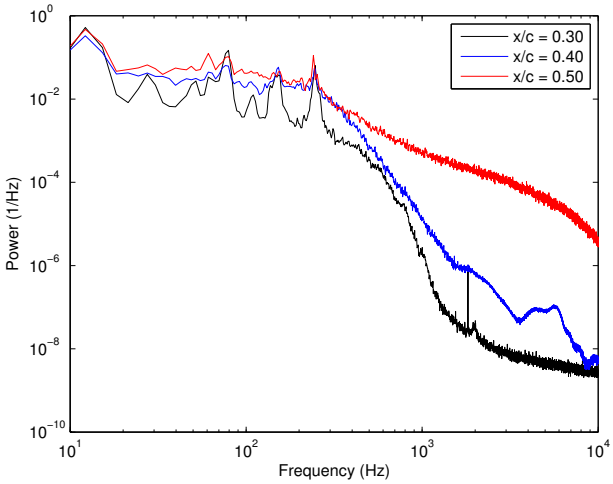


**Fig. 17** Fluctuating-velocity spectra, $Re_c = 1.6 \times 10^6$, [12|6.3|2.8] roughness.

The velocity profiles for this case are similar to the lower Reynolds number case. The overall disturbance amplitudes are higher compared to the lower Reynolds number case. This is to be expected from LST. The maximum disturbance amplitude shown in Fig. 18 increases significantly from $x/c = 0.30$ to $x/c = 0.40$, almost doubling. However, subsequent chordwise measurements show a decreasing maximum disturbance amplitude, but a broader range of higher values across the boundary layer.

The influence of DRE height on the unsteady disturbance profile in the travelling-wave pass-

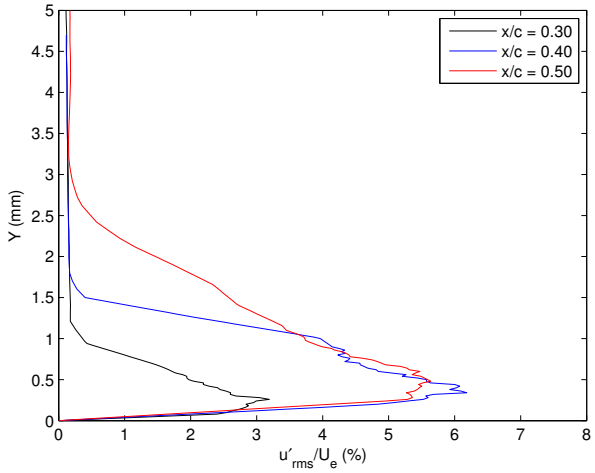


**Fig. 18** Unsteady disturbance profiles in the travelling-wave passband (50 – 500 Hz), $Re_c = 1.6 \times 10^6$, [12|6.3|2.8] roughness.

band is shown in Fig. 19. As for the lower Reynolds number case, there is an increase in the maximum disturbance amplitude, however the magnitude of this increase is not as large.

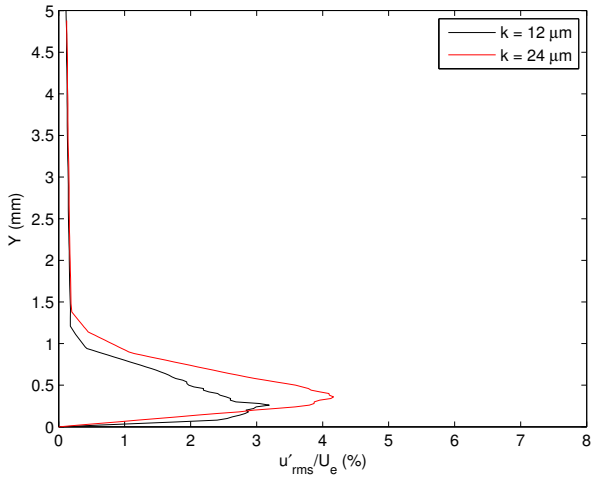


**Fig. 19** Unsteady disturbance profiles in the travelling-wave passband (50 – 500 Hz), $Re_c = 1.6 \times 10^6$, x/c = 0.30.

Figure 20 compares the influence of roughness height on the fluctuating-velocity spectrum. As for the lower Reynolds number case, there appears to be a broader distribution of power across the frequency range.

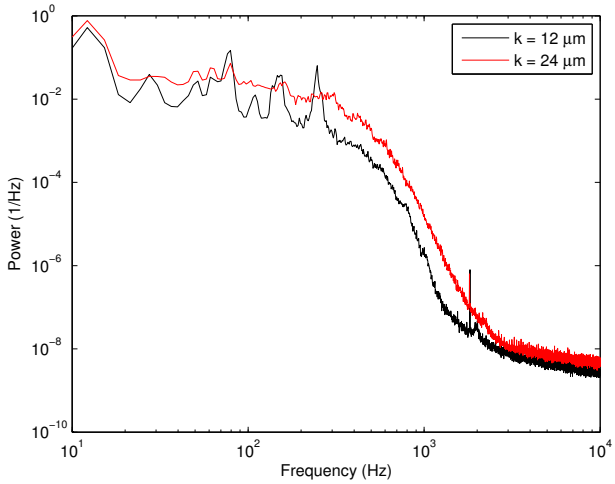


**Fig. 20** Fluctuating-velocity spectra, $Re_c = 1.6 \times 10^6$, x/c = 0.30.

## 6 Summary and conclusions

In this paper an overview of initial swept-wing experiments is provided. The aim is to document the flow quality of the wind tunnel facility used for the experiment, provide details of the experimental setup, establish the test conditions and document initial findings on the effects of surface roughness in a moderate-disturbance facility through flow visualisation and boundary-layer hot-wire measurements.

Free-stream measurements were carried out to evaluate the flow quality of the wind tunnel using hot-wire anemometry. It was determined that $u'_{rms}/U_\infty = 0.14\%$ and $v'_{rms}/U_\infty = 0.20\%$. A sound/vorticity separation technique was implemented using two hot wires separated by a large spanwise distance, but in the same streamwise plane: little correlation was seen between the two signals, implying that the measured disturbance intensity is mainly due to vortical disturbances.

To aid in the design of the swept-wing experiment, linear stability calculations were performed using experimentally determined pressure distributions at two chord Reynolds numbers: $Re_c = 1.3 \times 10^6$ and $Re_c = 1.6 \times 10^6$. The critical crossflow wavenumber was determined to be around 1000 /m. Critical travelling wave frequencies were determined to be between 200 Hz – 400 Hz.

Flow visualisation measurements reveal that for the baseline, clean leading-edge case, impressions were made by the stationary crossflow vortex on the surface of the wing, with a wavelength of approximately 6 mm; this agrees well with the linear stability predictions. For $Re_c = 1.3 \times 10^6$ transition was seen to arise in the region of adverse-pressure gradient toward the trailing edge of the wing, suggesting that the growth of the crossflow instability is weak and that T-S instabilities lead to transition. On insertion of DRE elements, spaced at the critical crossflow wavelength, transition was seen to move upstream. For an element height $k = 12$ $\mu$m transition is at $x/c = 0.60$ and appears to be stationary crossflow dominated. For $k = 24$ $\mu$m transition moves further upstream to $x/c = 0.50$, still appearing to be stationary crossflow dominated, though the stationary vortex striations are less distinct. For $Re_c = 1.6 \times 10^6$, a saw-tooth transition front was seen to arise between 55 – 60% chord, indicative of stationary crossflow dominated transition. On additional application of DRE layers, transition moved further upstream to $x/c = 0.50$ for $k = 12$ $\mu$m and $x/c = 0.40$ for $k = 24$ $\mu$m. As for the lower Reynolds number case at the higher DRE height, the stationary vortex striations are less obvious, and may be due to travelling waves becoming more dominant.

On considering the measured free-stream disturbance intensities and LST calculations at the Reynolds numbers of interest, travelling waves might be the expected dominant crossflow mode. Flow visualisation and mean-velocity-profile measurements suggest, however that at $Re_c = 1.3 \times 10^6$ the stationary modes dominate. Velocity spectra show a high-frequency peak characteristic of a secondary-instability. Increasing roughness height does show an increase in unsteady disturbance amplitude, implying that height does not only affect the stationary crossflow mode, but also the travelling crossflow. The low-roughness height case shows distinct peaks corresponding to the primary travelling wave mode; increasing the roughness height broadens out these peaks and gives rise to a higher distribution of energy, suggesting that the free-stream turbulence may be exciting the travelling crossflow modes across multiple frequencies. The same characteristic features are prevalent at $Re_c = 1.6 \times 10^6$, though the unsteady disturbance amplitudes are higher and the high-frequency peak attributed to a secondary instability is even more distinct.

These observations agree with previous work, in that turbulence intensity alone is not the only receptivity parameter that determines which crossflow mode will ultimately be prevalent, and that roughness is an important parameter for the growth of travelling waves as well as stationary crossflows. The work of [Dow12] showed that sub-critically spaced elements placed in a moderate disturbance environment lead to travelling wave dominance, with roughness height having little effect; the hypothesis there was that it is the increased number of element-induced vortices that led to travelling wave dominance. The work here shows that roughness height does play a crucial role, which should be investigated further.

Future investigations will explore the role of roughness configuration on crossflow transition in a moderate disturbance environment. Data from the configurations presented here will be supplemented with spanwise hot-wire measurements. The effects of spanwise density of DRE elements will be explored further along with the influence of roughness height. Future studies will also examine the role that anisotropy of free-stream turbulence plays, with further studies of free-stream turbulence for the present tunnel configuration, and after insertion of a turbulence reducing grid.

## Acknowledgements

We are grateful to Prof. Ahmed Naguib for providing an optimal filtering code used for the separation of sound/vortical disturbances. We are indebted to Airbus for providing the AERAST wing model and sharing details of the china clay sublimation technique. The authors thank EPSRC for funding the research through the LFC-UK grant, EP/I037946.

## References


[Bip99] H. Bippes. Basic experiments on transition in three-dimensional boundary layers dominated by crossflow instability. *Progress in Aerospace Sciences*, pages 363–412, 1999.

[Bru96] H. H. Bruun. *Hot-Wire Anemometry Principles and Signal Analysis*. Oxford Science, 1996.

[CRS96] R. B. Carrillo, M. S. Reibert, and W. S. Saric. Distributed-roughness effects on stability and transition in swept-wing boundary layers. CR 203580, NASA, 1996.

[CSR08] A. Carpenter, W.S. Saric, and H.L. Reed. Laminar flow control on a swept wing with distributed roughness. In *26th AIAA Applied Aerodynamics Conference*, 2008.

[DB96] H. Deyhle and H. Bippes. Disturbance growth in an unstable three-dimensional boundary layer and its dependence on environmental conditions. *Journal of Fluid Mechanics*, 316:73–113, 1996.

[Dow12] R. S. Downs. *Environmental Influences on Crossflow Instability*. PhD thesis, Texas A&M University, 2012.

[DW13] R. S. Downs and E. B. White. Free-stream turbulence and the development of cross-flow disturbances. *Journal of Fluid Mechanics*, 735:347 – 380, 2013.

[Gre08] J. E. Green. Laminar flow control - back to the future. Number 2008-3738 in Paper. AIAA, 2008.

[HS11] L. E. Hunt and W. S. Saric. Boundary-layer receptivity of three-dimensional roughness arrays on a swept wing. Number 2011-3881. AIAA Paper, 2011.

[Hun11] L. E. Hunt. *Boundary-Layer Receptivity to Three-Dimensional Roughness Arrays on a Swept-Wing*. PhD thesis, Texas A&M University, 2011.

[KFA11] T. Kurian, J. H. M. Fransson, and P. H. Alfredsson. Boundary layer receptivity to free-stream turbulence and surface roughness over a swept flat plate. *Physics of Fluids*, 23(3), 2011.

[LJ02] B. Lindgren and A.V. Johansson. Evaluation of the flow quality in the mtl wind tunnel. Technical Report TRITA-MEK 2002:13, Royal Institute of Technology, Department of Mechanics, KTH, SE-100 44 Stockholm, Sweden, 2002.

[MA13] M. S. Mughal and R. Ashworth. Uncertainty quantification based receptivity modelling of crossflow instabilities induced by distributed surface roughness in swept wing boundary layers. Number AIAA-2013-3106, 2013.

[Mac84] L. M. Mack. Boundary-layer linear stability theory. Technical Report Rep. 709, AGARD, 1984.

[NGW96] A.M. Naguib, S.P. Gravante, and C.E. Wark. Extraction of turbulent wall-pressure time-series using an optimal filtering scheme. *Experiments in Fluids*, pages 14–22, 1996.

[SAB10] L. Schrader, S. Amin, and L. Brandt. Transition to turbuelnce in the boundary layer over a smooth and rough swept plate exposed to free-stream turbulence. *Journal of Fluid Mechanics*, 646:297–325, 2010.

[SBH09] L. Schrader, L. Brandt, and D. S. Henningson. Receptivity mechanisms in three-dimensional boundary-layer flows. *Journal of Fluid Mechanics*, 618:209 – 241, 2009.

[SRW03] W.S. Saric, H.L. Reed, and E.B. White. Stability and transition of three-dimensional boundary layers. *Journal of Fluid Mechanics*, 35:413–440, 2003.

[SS09] R. Sunderland and D. Sawyers. Evaluation of AERAST large scale wind-tunnel test results. Technical Report RP0905747, Airbus, 2009.

[TFY07] E. Tropea, J. Foss, and A. Yarin. *Springer Handbook of Experimental Fluid Mechanics*, chapter Wall-Bounded Shear Flows. Springer, 2007.

[THH12] D. Tempelmann, A. Hanifi, and D. S. Henningson. Swept-wing boundary-layer receptivity. *Journal of Fluid Mechanics*, 700:490 – 501, 2012.

[WK02] P. Wassermann and M. Kloker. Mechanism and passive control of crossflow-vortex-induced transition in a three-dimensional boundary layer. *Journal of Fluid Mechanics*, 456:49–84, 2002.

[WK03] P. Wassermann and M. Kloker. Transition mechanisms induced by tavelling crossflow vortices in a three-dimensional bounday layer. *Journal of Fluid Mechanics*, 483:67 – 89, 2003.

[WS05] E.B. White and W.S. Saric. Secondary instability of crossflow vortices. *Journal of Fluid Mechanics*, 525:275–308, 2005.

[WSGG] E. B. White, W. S. Saric, R. D. Gladden, and P. M. Gabet. Stages of swept-wing transition. Number 2001-0271. *AIAA* Paper.

## 7 Contact author email address

t.saeed@imperial.ac.uk

## Copyright statement